Coupling Mechanical and Electrical Properties in Spin Crossover Polymer Composites

Sylvain Rat, Mario Piedrahita-Bello, Lionel Salmon, Gábor Molnár, Philippe Demont,* and Azzedine Bousseksou**

Spin crossover particles of formula $[Fe\{(Htrz)_2(trz)\}_{0.9}(NH_2\text{-}trz)_{0.3}](BF_4)_{1.1}$ and average size of 20 nm ± 8 nm are homogeneously dispersed in poly(vinylidene fluoride-co-trifluoro-ethylene), P(VDF-TrFE), and poly(vinylidene fluoride) (PVDF) matrices to form macroscopic (cm-scale), freestanding, and flexible nanocomposite materials. The composites exhibit concomitant thermal expansion and discharge current peaks on cycling around the spin transition temperatures, i.e., new "product properties" resulting from the synergy between the particles and the matrix. Poling the P(VDF-TrFE) (70–30 mol%) samples loaded with 25 wt% of particles in 18 MV m^{-1} electric field results in a piezoelectric coefficient $d_{33} = -3.3$ pC N^{-1}. The poled samples display substantially amplified discharges and altered spin transition properties. Analysis of mechanical and dielectric properties reveals that both strain (1%) and permittivity (40%) changes in the composite accompany the spin transition in the particles, giving direct evidence for strong electromechanical couplings between the components. These results provide a novel route for the deployment of molecular spin crossover materials as actuators in artificial muscles and generators in thermal energy harvesting devices.

Molecular actuators are a class of switchable molecules, which are able to transduce thermal, optical, electrical, or chemical stimuli into useful mechanical work on their surroundings.[1–8] Beyond purely mechanical applications, these compounds represent a particularly attractive scope for the development of chemomechanical, biomimetic, and other complex systems combining built-in actuator, sensor, and energy harvesting functions, which is the key requirement for achieving highly integrated, versatile, and adaptive actuator systems.[9–12]

Among these smart molecules, the important reversible volume change of molecular spin-crossover (SCO) switches has been successfully exploited in the past years to develop mechanical actuators[13,14] integrated into microelectromechanical systems[15–18] as well as into macroscopic "artificial muscles."[14,19] For these applications, however, the use of electrical stimuli to control (read/write) the spin-state of the system would provide a great advantage due to the easier size reduction and better compatibility with current technology.[20] Unfortunately, bulk SCO solids are basically low loss dielectric materials characterized by rather low electrical conductivity and permittivity values.[20] In order to confer them with more appealing electrical properties, hybrid materials comprising both SCO and electroactive bricks have been recently synthesized. Notably, this was achieved by cocrystallizing SCO complexes and conducting molecular species in the same crystal lattice. Most of these compounds exhibit either SCO or semiconducting behavior or both at the same time, but a clear coupling between the two phenomena has been reached only in a few cases.[21,22] On the other hand, electroactive hybrid SCO systems have been also achieved by means of interfacial coupling in thin film heterostructures.[23] New electrical behavior is also seen in polymer composites of SCO particles. The benchmark SCO complex $[Fe(Htrz)_2(trz)](BF_4)$ (Htrz = 1H-1,2,4-triazole) displays a conductance switching of several orders of magnitude, but at very low conductivity levels (≈10^{-8}–10^{-10} S cm^{-1}).[24] When this complex is incorporated in a piezoresistive polymer matrix, such as polypyrrole, the composite material exhibits a 60% conductivity switching between 3.10^{-2} and 6.10^{-2} S cm^{-1} as a result of the interplay between the SCO and piezoresistive properties.[25]

Here, we report on the synthesis of a new type of versatile ferroelectric polymer—SCO nanocomposite with the aim to demonstrate novel electro–mechanical effects with particular relevance for mechanical actuation and energy harvesting devices. Among the available ferroelectric polymers, we have chosen two different polymer matrices, poly(vinylidene fluoride) (PVDF) and its copolymer P(VDF-TrFE) 70–30% mol (**Figure 1**a), which are probably the most attractive for their good piezo- and pyroelectric responses as well as for their easy and versatile processing.[26] The choice of the SCO complex used in this study was imposed by the relatively narrow temperature window of ≈303–363 K (depending on the exact composition) wherein the polymers can be conveniently used.

S. Rat, M. Piedrahita-Bello, Dr. L. Salmon, Dr. G. Molnár, Dr. A. Bousseksou
LCC
CNRS & University of Toulouse (UPS, INPT)
205 route de Narbonne, 31077 Toulouse, France
E-mail: gabor.molnar@lcc-toulouse.fr;
azzedine.bousseksou@lcc-toulouse.fr
Prof. P. Demont
CIRIMAT
CNRS & University of Toulouse (UPS, INPT)
118 Route de Narbonne, 31062 Toulouse, France
E-mail: philippe.demont@univ-tlse3.fr

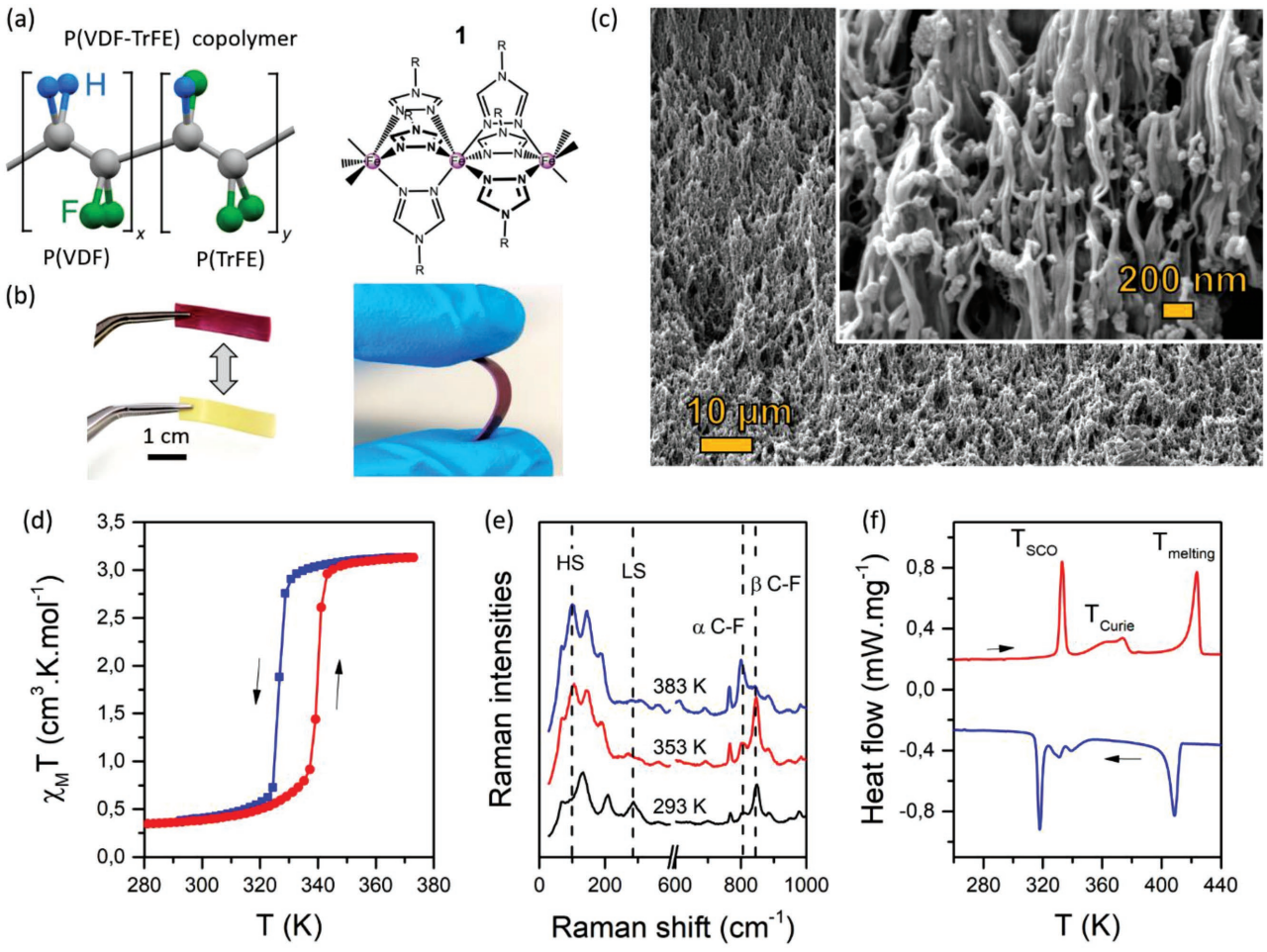

Figure 1. Characterization of the P(VDF-TrFE)/SCO composite: a) Schemes of the copolymer and SCO complex **1**. b) Photographs of the flexible, free-standing film in the LS (violet) and HS (yellow) states. c) Representative SEM images of the composite cross-section. d) Variable-temperature magnetic susceptibility (per mol Fe in the composite) on heating and cooling. e) Variable temperature Raman spectra in the LS (293 K) and HS (353 K) states as well as above the Curie temperature (383 K). Markers of the different phases of the complex (HS/LS) and of the polymer (α/β) are shown by dotted lines. f) DSC thermograms on heating and cooling. The spin transition, Curie, and melting peaks are clearly discernible.

Indeed, out of this window the mechanical and electrical properties of P(VDF-TrFE) change due to the proximity of the Curie temperature in the high temperature range and relaxation phenomena at low temperatures.[27] It may be worth to note here that for "synchronizing" the properties of the two components, one might either tune the ligand stoichiometry of the SCO complex,[28] which we did in this work, or modify the polymer properties, for example, by adjusting the VDF-TrFE ratio.[26]

Nanoparticles of $[Fe\{(Htrz)_2(trz)\}_{0.9}(NH_2\text{-}trz)_{0.3}](BF_4)_{1.1}$ **1** (Figure 1; Supporting Information) with a mean size of 20 ± 8 nm, synthetized using highly concentrated solutions of reagents, exhibit thermal spin transition around 335 K with a hysteresis loop. Freestanding films of the P(VDF-TrFE)/**1** nanocomposite were reproducibly prepared (five identical samples) by using a drop-cast approach (see Supporting Information for details). The amount of **1** in the polymer matrix was ≈25 wt% determined by Fe inductively coupled plasma-atomic emission spectroscopy (ICP-AES) analysis. Scanning electron microscopy (SEM) and atomic force microscopy images revealed a homogeneous dispersion of nanoparticles inside the fibrous-like polymer structure (Figure 1c; see also Figure S2 in the Supporting Information), approaching the morphology of an ideal 0–3 connectivity composite material.[29] It should be noted that synthesis conditions were not arbitrary, but the result of a fastidious optimization of composite preparation parameters (see Supporting Information). To demonstrate the versatility of our approach we also synthesized and characterized electrical–mechanical properties of composites of **1** in PVDF matrix and we obtained preliminary data with composites of the SCO complex $[Fe(HB(tz)_3)_2]$ (tz = triazolyl) in P(VDF-TrFE), leading to similar results (see Supporting Information). Control experiments using the pure polymers are also reported in the Supporting Information.

The spin transition in the nanocomposite P(VDF-TrFE)/**1** was obvious from its marked thermochromism between the violet low spin (LS) and the yellow high spin (HS) states (Figure 1b). Variable-temperature magnetic susceptibility (Figure 1d) revealed a virtually complete SCO with transition temperatures around $T_{1/2}$ = 340 K and $T_{1/2}$ = 327 K on heating and cooling, respectively. The hysteresis width in the composite (13 K) is notably larger in comparison with that of the particles alone (8 K; see

Figures S9 and S10 in the Supporting Information) due, possibly, to elastic confinement effects of the matrix, though other reasons (e.g., solvent effect) cannot be excluded. The spin transition in the composite is reproducible over several thermal cycles, except the first heating curve (see Figure S10 in the Supporting Information). This irreversibility of the first heating transition is well-known for many SCO materials ("run-in" phenomenon) and can be attributed to various phenomena such as the loss of solvents and/or particle morphology changes, and/or polymorphism.[30,31] For this reason, we show material properties observed during the second (stable) thermal cycle, except otherwise stated.

The spin transition and other thermally induced phenomena in the composite were further investigated by Raman microspectroscopy and differential scanning calorimetry (DSC). The Raman spectra of the composite were found homogenous and consist of the superposition of the spectra of **1** and P(VDF-TrFE) (see Figure 1e; Figures S12–14 in the Supporting Information). At room temperature the well-known fingerprints of the LS phase of **1** (131, 207 and 288 cm^{-1})[32] and the so-called β phase of the P(VDF-TrFE) matrix (840 cm^{-1})[33] can be clearly discerned. When the temperature is increased above ≈340 K a decrease of the intensity of the LS markers is observed while other peaks, characteristic of the HS phase, emerge around 103, 144, and 190 cm^{-1}. In agreement with the magnetic data, the spin transition appears virtually complete in both directions. On further heating above the Curie temperature of P(VDF-TrFE) (≈360 K) the intensity of the Raman marker of the β polar phase decreases, while that of the α paraelectric phase (794 cm^{-1}) increases. The DSC analysis (Figure 1f) shows, in good agreement with the magnetic and Raman data, endo- and exothermic peaks, which accompany the spin transition around 334 and 318 K, respectively. The associated transition enthalpy (ΔH = 20 kJ mol^{-1}) and entropy (ΔS = 60 J K^{-1} mol^{-1}) changes are comparable with those observed for the pure complex (see Figure S17 in the Supporting Information). The ferro/paraelectric transition is characterized by two peaks in the DSC thermograms (T_{C1} = 362/327 K, T_{C2} = 373/338 K upon heating/cooling) indicating the coexistence of two ferroelectric phases.[34] It is important to note also that the Curie and melting temperatures and associated enthalpy changes of the polymer matrix (corrected for the wt%) are not considerably altered by the SCO filler (see Figures S16 and S17 in the Supporting Information), which indicates that the crystallinity of the polymer is preserved in the composite.

The spin transition in **1** is associated with a substantial spontaneous volumetric strain of ≈10% (see the powder XRD data in Figure S3 in the Supporting Information).[35,36] If this mechanical strain is efficiently transferred to the electroactive polymer matrix a change of the polarization level of this latter should take place due to the electro–mechanical coupling. Under short-circuit conditions one would therefore expect a transient current flow during the spin transition. The key result of this work is the repeated experimental observation of this "pseudo-pyroelectric" effect in the composite materials in the form of discharge current peaks when submitted to temperature changes around the spin transition temperatures (see **Figure 2**a; Figure S10 in the Supporting Information). The as-synthesized composite has a random organization of ferroelectric domains and the net macroscopic polarization is zero. Despite this fact, small, but clearly discernible discharge currents were observed upon the spin transition even in the nonpolarized material. Poling of samples was undertaken at 293 K by applying several cycles of a sinusoidal electric field (100 mHz) with amplitudes up to 13.6 and 18 MV m^{-1}. The resulting piezoelectric coefficient d_{33}, which provides direct information on the mechanical to electrical (and vice-versa) conversion efficiency, was −2.3 and −3.3 pC N^{-1}, respectively. These values are reduced with respect to the −20 pC N^{-1} measured for the pure P(VDF-TrFE). Smaller values of d_{33} are generally observed in composites with nonferroelectic loads.[37] This decrease of d_{33} may be attributed to the action of depoling field generated by space charges on the particles during poling. Another explanation is a disruption of the connectivity of the polymer matrix related to the existence of particle agglomerates. We can recall here that the piezoelectric coefficient in ferroelectric polymers is, for the most part, linearly controlled by the polarization and the compressibility (secondary piezoelectric effect), unlike ferroelectric ceramics where the primary piezoelectric effect at constant volume dominates. In the composites both parameters are lower. In particular the reduced breakdown voltage allows for smaller sample polarization. Using different sample preparation (thickness, annealing, etc.) we were able to increase d_{33} up to −9.0 pC N^{-1} (with a 24 MV m^{-1} applied field for a 150 μm thickness), which was also stable in time (month scale) indicating ferroelectric properties. However, this was achieved at the expense of mechanical properties (fragility) thus we were not able to pursue a full characterization with this sample. Following the poling process, the composite was cycled between 260 and 360 K without any applied voltage. The resulting thermally stimulated current curves reveal pronounced discharge current peaks around the spin transition temperatures, which are significantly enhanced with respect to the nonpoled sample (see inset in Figure 2a).

It is important to remark that despite some resemblance with ordinary pyroelectric effects, the measured zero-bias current in Figure 2a has a different origin in our material, which is obvious from the fact that the sign of the current is not inversed between heating and cooling. (N.B. Actually, upon the first thermal cycle we could observe the usual current sign inversion (see Figure S20a in the Supporting Information), but not in further cycles, which we attribute to the fact that during the first heating the spin transition temperature is higher and overlaps with the Curie transition.) Another interesting observation is the downshift of the spin transition temperature in the cooling mode from ≈326 K (nonpolarized sample) to 320 K (sample poled at 18 MV m^{-1}) as shown in the insert of Figure 2a. This small electric field effect on the SCO was repeatedly confirmed (see Figures S20b and S26 in the Supporting Information) and denotes a possible field-induced stabilization of the HS state, as a consequence of the polarization of the polymer matrix, which is a very promising property and calls for further studies.

To better understand the remarkable electromechanical coupling between the components, both the P(VDF-TrFE) and PVDF composites were further investigated by means of variable temperature dynamical mechanical analysis (DMA) and broadband dielectric spectroscopy (BDS). Figure 2b shows the temperature dependence of the thermal expansion coefficient α_L under an applied static tensile stress. Far from the spin transition, one can observe a virtually constant value of α_L (slightly

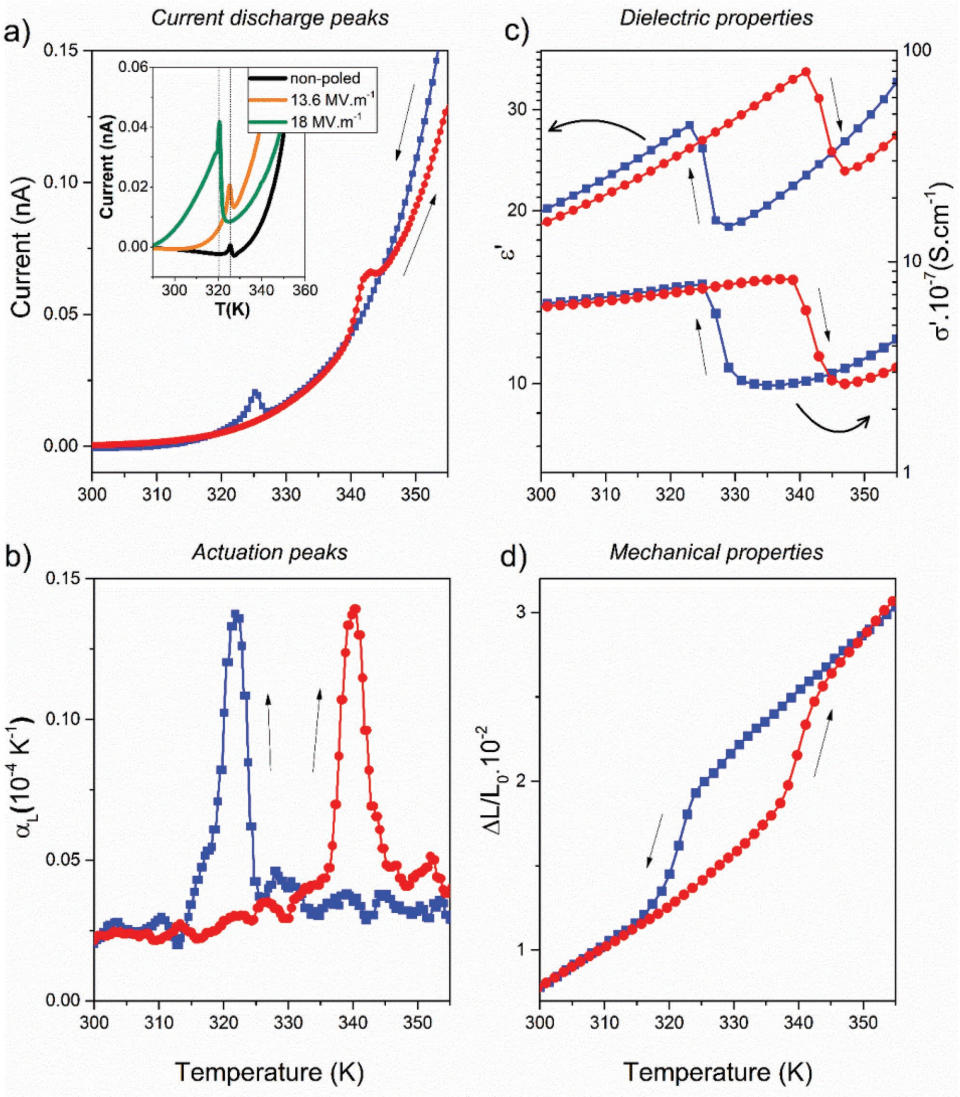

Figure 2. Electrical and mechanical properties of the P(VDF-TrFE)/SCO composite: a) Short-circuit current under zero applied bias on heating and cooling at rates of ±2 K min^{-1}. Measurements were done after poling the sample in a 13.6 MV m^{-1} electrical field. The inset shows the modulation of the amplitude and temperature of the discharge current peak (cooling mode) controlled by the initial polarization. b) Temperature dependence of the linear expansion coefficient. c) Dielectric permittivity and electrical conductivity at 100 kHz as a function of the temperature. d) Temperature dependence of the engineering strain under tensile testing. Arrows indicate heating and cooling.

different in the two spin states). When going from the LS (HS) to the HS (LS) phase a divergence of α_L occurs corresponding to the abrupt elongation (contraction) of the sample (Figure 2d). This actuation peak associated with the SCO is the second key outcome of our approach. Taking into account the ≈25 wt% particle load, the 1% linear strain of the composite is in line with the ≈10% volume expansion of **1** upon the SCO.

The strong mechanical coupling between the particles and the matrix is also clearly seen in the loss tangent tan δ (Figure S21c, Supporting Information) and loss modulus E'' (Figure S21b, Supporting Information) behavior, which exhibit pronounced dissipation peaks around the spin transition temperatures. Such anelastic phenomena are typical in materials with first-order phase transitions and can be associated with the internal frictions during the nucleation and domain growth process.[38,39] In addition to this transitory phenomenon, the loss modulus exhibits also a persisting decrease in the HS phase, particularly pronounced in the PVDF composite (≈40%; see Figure S25c in the Supporting Information), which is indicative of a less viscoelastic behavior with respect to the LS phase. This is also in line with the increase of the storage modulus E' in the HS form (by ≈8%, see Figure S21a in the Supporting Information). The temperature dependence of the dielectric permittivity of the composite is shown Figure 2c. The room temperature value of $\varepsilon' = 17$ is similar to that of the pure P(VDF-TrFE) polymer, but on heating across the spin transition temperature it drops (reversibly) by ≈40% indicating a significantly reduced storage capacity of the material in the HS state. On the other hand, owing to the highly insulating nature of **1** the conductivity of the composite remains very low in both spin

states (< 10^{-6} S cm^{-1}), which is a useful property as it allows to keep small the leakage currents in the composite material. In fact, the observation of such important discharge peaks would be impossible with a conducting filler. Hence, the poor conductivity, considered in general as a drawback for SCO compounds, becomes here a key advantage. Overall this DMA and BDS analysis of the composites reveals that the excellent electromechanical properties of the P(VDF-TrFE) and PVDF (see Figures S24 and S25 in the Supporting Information) matrices have been preserved to a large extent in the composite material. The DMA results confirm the effective strain coupling between the SCO particles and the polymer matrix providing support for our initial hypothesis on the mechanical origin of the "anomalous" discharge current peaks at the spin transition. On the other hand, the BDS data reveal also a strong modulation of the permittivity of the composite between the two spin states, which contributes obviously also to the "pseudo-pyroelectric" currents. Theoretical modeling will be necessary to disentangle these contributions.

In summary, we succeeded in synthesizing high quality, homogenous P(VDF-TrFE) and PVDF composites of $[Fe\{(Htrz)_2(trz)\}_{0.9}(NH_2\text{-}trz)_{0.3}](BF_4)_{1.1}$ spin transition nanoparticles in a reproducible manner allowing us to obtain flexible, freestanding, macroscopic (cm scale) objects displaying original electro–mechanical synergies between the two components. In particular, this coupling leads to concomitant macroscopic thermal expansion and electrical discharge peaks at the spin transition. In addition the dielectric permittivity exhibits also an important hysteresis. These new properties provide a scope for the deployment of spin transition materials as actuators in artificial muscles and generators in thermal energy harvesting devices. The key advantages of our composite-SCO approach (vs the pure polymers) for these applications are the possibility to: (1) use very small temperature excursions, restricted to a narrow temperature window around the spin transition;[40] (2) use different SCO compounds to adjust this window to the targeted application;[28] (3) obtain actuation/discharge peaks, which is particularly advantageous for applications needing high power.[41] We believe this concept of coupling the spontaneous strain of a first order phase transition with piezo/pyro/ferro-electric matrices should be easily extended to other material combinations providing thus considerable versatility for the engineering of physico–chemical properties of electroactive polymers. Further systematic studies, including different particle sizes/shapes and polymer compositions, will be the scope of future work.

Supporting Information

Supporting Information is available from the Wiley Online Library or from the author.

Acknowledgements

The work was supported by the ANR NANOHYBRID project (ANR-13-BS07-0020-01). S.R. thanks the French Ministry of Research for a PhD grant.

Conflict of Interest

The authors declare no conflict of interest.

Keywords

electromechanical effects, molecular switches, polymer composites, spin-crossover

Received: September 13, 2017
Revised: November 14, 2017
Published online:

[1] W. R. Browne, B. L. Feringa, *Nat. Nanotechnol.* **2006**, *1*, 25.
[2] F. Niess, V. Duplan, J.-P. Sauvage, *Chem. Lett.* **2014**, *43*, 964.
[3] M. D. Manrique-Juárez, S. Rat, L. Salmon, G. Molnár, C. M. Quintero, L. Nicu, H. J. Shepherd, A. Bousseksou, *Coord. Chem. Rev.* **2016**, *308*, 395.
[4] V. Balzani, A. Credi, M. Venturi, *Molecular Devices and Machines: Concepts and Perspectives for the Nanoworld*, Wiley-VCH, Weinheim, Germany **2008**.
[5] P. Naumov, S. Chizhik, M. K. Panda, N. K. Nath, E. Boldyreva, *Chem. Rev.* **2015**, *115*, 12440.
[6] J. M. Abendroth, O. S. Bushuyev, P. S. Weiss, C. J. Barrett, *ACS Nano* **2015**, *9*, 7746.
[7] A. Coskun, M. Banaszak, R. D. Astumian, J. F. Stoddart, B. A. Grzybowski, *Chem. Soc. Rev.* **2012**, *41*, 19.
[8] T. Ube, T. Ikeda, *Angew. Chem., Int. Ed.* **2014**, *53*, 10290.
[9] P. Egan, R. Sinko, P. R. LeDuc, S. Keten, *Nat. Commun.* **2015**, *6*, 7418.
[10] M. A. McEvoy, N. Correll, *Science* **2015**, *347*, 1261689.
[11] S. Kim, C. Laschi, B. Trimmer, *Trends Biotechnol.* **2013**, *31*, 287.
[12] J. D. Madden, *Science* **2007**, *318*, 1094.
[13] H. J. Shepherd, I. A. Gural'skiy, C. M. Quintero, S. Tricard, L. Salmon, G. Molnár, A. Bousseksou, *Nat. Commun.* **2013**, *4*, 2607.
[14] I. A. Gural'skiy, C. M. Quintero, J. S. Costa, P. Demont, G. Molnár, L. Salmon, H. J. Shepherd, A. Bousseksou, *J. Mater. Chem. C* **2014**, *2*, 2949.
[15] M. D. Manrique-Juarez, S. Rat, F. Mathieu, D. Saya, I. Séguy, T. Leïchlé, L. Nicu, L. Salmon, G. Molnár, A. Bousseksou, *Appl. Phys. Lett.* **2016**, *109*, 061903.
[16] Y.-C. Chen, Y. Meng, Z.-P. Ni, M.-L. Tong, *J. Mater. Chem. C* **2015**, *3*, 945.
[17] M. Urdampilleta, P.-H. Ducrot, D. Rosario-Amorin, A. Mondal, M. Rouzières, P. Dechambenoit, C. Mathonière, F. Mathieu, I. Dufour, C. Ayela, R. Clérac, *ArXiv:170101341* **2017**.
[18] M. D. Manrique-Juárez, F. Mathieu, V. Shalabaeva, J. Cacheux, S. Rat, L. Nicu, T. Leïchlé, L. Salmon, G. Molnár, A. Bousseksou, *Angew. Chem., Int. Ed.* **2017**, *129*, 8186.
[19] S. Rat, V. Nagy, I. Suleimanov, G. Molnár, L. Salmon, P. Demont, L. Csóka, A. Bousseksou, *Chem. Commun.* **2016**, *52*, 11267.
[20] C. Lefter, V. Davesne, L. Salmon, G. Molnár, P. Demont, A. Rotaru, A. Bousseksou, *Magnetochemistry* **2016**, *2*, 18.
[21] M. Nihei, N. Takahashi, H. Nishikawa, H. Oshio, *Dalton Trans.* **2011**, *40*, 2154.
[22] K. Takahashi, H.-B. Cui, Y. Okano, H. Kobayashi, H. Mori, H. Tajima, Y. Einaga, O. Sato, *J. Am. Chem. Soc.* **2008**, *130*, 6688.
[23] X. Zhang, T. Palamarciuc, J.-F. Létard, P. Rosa, E. Vega Lozada, F. G. Torres, P. Rosa, B. Doudin, P. Dowben, *Chem. Commun.* **2014**, *50*, 2255.

[24] A. Rotaru, I. A. Gural'skiy, G. Molnár, L. Salmon, P. Demont, A. Bousseksou, *Chem. Commun.* **2012**, *48*, 4163.
[25] Y.-S. Koo, J. R. Galán-Mascarós, *Adv. Mater.* **2014**, *26*, 6785.
[26] P. Martins, A. C. Lopes, S. Lanceros-Mendez, *Prog. Polym. Sci.* **2014**, *39*, 683.
[27] G. Teyssèdre, C. Lacabanne, *Ferroelectrics* **1995**, *171*, 125.
[28] J. Kröber, E. Codjovi, O. Kahn, F. Groliere, C. Jay, *J. Am. Chem. Soc.* **1993**, *115*, 9810.
[29] E. K. Akdogan, M. Allahverdi, A. Safari, *IEEE Trans. Ultrason. Ferroelectr. Freq. Control* **2005**, *52*, 746.
[30] L. G. Lavrenova, O. G. Shakirova, *Eur. J. Inorg. Chem.* **2013**, 670.
[31] M. D. Manrique-Juárez, I. Suleimanov, E. M. Hernández, L. Salmon, G. Molnár, A. Bousseksou, *Materials* **2016**, *9*, 537.
[32] N. Ould Moussa, D. Ostrovskii, V. M. Garcia, G. Molnár, K. Tanaka, A. B. Gaspar, J. A. Real, A. Bousseksou, *Chem. Phys. Lett.* **2009**, *477*, 156.
[33] K. Tashiro, M. Kobayashi, *Polymer* **1988**, *29*, 426.
[34] H. Tanaka, H. Yukawa, T. Nishi, *Macromolecules* **1988**, *21*, 2469.
[35] A. Grosjean, P. Négrier, P. Bordet, C. Etrillard, D. Mondieig, S. Pechev, E. Lebraud, J.-F. Létard, P. Guionneau, *Eur. J. Inorg. Chem.* **2013**, 796.
[36] I. Suleimanov, J. Sanchez Costa, G. Molnar, L. Salmon, I. O. Fritsky, A. Bousseksou, *Fr. Ukr. J. Chem.* **2015**, *3*, 66.
[37] T. H. L. Nguyen, L. Laffont, J.-F. Capsal, P.-J. Cottinet, A. Lonjon, E. Dantras, C. Lacabanne, *Mater. Chem. Phys.* **2015**, *153*, 195.
[38] J. X. Zhang, P. C. W. Fung, W. G. Zeng, *Phys. Rev. B* **1995**, *52*, 268.
[39] R. B. Pérez-Sáez, V. Recarte, M. L. Nó, J. San Juan, *Phys. Rev. B* **1998**, *57*, 5684.
[40] S. R. Hunter, N. V. Lavrik, T. Bannuru, S. Mostafa, S. Rajic, P. G. Datskos, *Proc. SPIE* **2011**, *8035*, 80350V.
[41] C. R. Bowen, J. Taylor, E. LeBoulbar, D. Zabek, A. Chauhan, R. Vaish, *Energy Environ. Sci.* **2014**, *7*, 3836.